Spatiotemporal learning in analog neural networks using spike-timing-dependent synaptic plasticity

Masahiko Yoshioka,[1] Silvia Scarpetta,[1,2,3] and Maria Marinaro[1,2,3]
[1]*Department of Physics, "E.R. Caianiello," University of Salerno, 84081 Baronissi SA, Italy*
[2]*INFN , 84100 Salerno SA, Italy*
[3]*IIASS, Vietri sul Mare, 84019 Vietri sul Mare SA, Italy*
(Received 17 July 2006; revised manuscript received 4 November 2006; published 29 May 2007)

Incorporating the spike-timing-dependent synaptic plasticity (STDP) into a learning rule, we study spatiotemporal learning in analog neural networks. First, we study learning of a finite number of periodic spatiotemporal patterns by deriving the dynamics of the order parameters. When a pattern is retrieved successfully, the order parameters exhibit periodic oscillation. Analyzing this oscillation of the order parameters, we elucidate the relation of the STDP time window to the properties of the retrieval state; the phase of the Fourier transform of the STDP time window determines the retrieval frequency and the time average of the STDP time window crucially affects the storage capacity. We also evaluate the stability of the order parameter oscillation and identify the retrieval state that is stable in single-pattern learning but unstable in multiple-pattern learning even when the retrieval state is independent of a pattern number. To examine the further applicability of the STDP-based learning rule, we also study learning of nonperiodic spatiotemporal Poisson patterns. Our numerical simulations demonstrate that the Poisson patterns are memorized successfully not only in analog neural networks but also in spiking neural networks.

DOI: 10.1103/PhysRevE.75.051917 PACS number(s): 87.18.Sn, 82.40.Bj, 05.50.+q, 87.10.+e

I. INTRODUCTION

There has been constant attention given to the relation of memory function of the brain to synapse plasticity. Thus, several efforts have been devoted to the analysis of theoretical models of associative memory neural networks [1–23]. In these studies of associative memories, neural networks are mostly modeled to memorize binary patterns $\xi_i^\mu = \pm 1$ $(i=1,\ldots,N,\ \mu=1,\ldots,P)$ with the application of the Hebb learning rule $J_{ij}=(1/N)\Sigma_\mu \xi_i^\mu \xi_j^\mu$. This typical Hebb learning rule is useful since it provides symmetric synapse connections (i.e., $J_{ij}=J_{ji}$). In spin neural networks, symmetric synapse connections ensure the existence of an energy function, which allows one to apply the sophisticated analytical methods in the equilibrium statistical mechanics to investigating neural networks [1]. In fact, Amit *et al.* have evaluated the energy function with the replica method and derived the storage capacity of symmetric spin neural networks [3]. Thanks to these advanced analyses we have seen great progress in the study of neural networks with symmetric synapse connections.

On the other hand, neural networks with asymmetric synapse connections remain less understood since an energy function is undefinable in most asymmetric neural networks. However, such neural networks without an energy function are essential for learning about spatiotemporal patterns since neural networks with an energy function, which eventually settle into an certain equilibrium state, are apparently incapable of retrieving dynamical spatiotemporal patterns. It is well known that a simple asymmetric modification of the Hebb learning rule $J_{ij}=(1/N)\Sigma_\mu \xi_i^{\mu+1} \xi_j^\mu$ realizes spatiotemporal learning in discrete-time neural networks with the synchronous update rule [4,5]. This modification of the Hebb learning rule is, however, useless in realistic neural networks based on continuous-time dynamics or the asynchronous update rule since continuous transition of sequential patterns in continuous-time dynamics is much more difficult to control than discrete transition of sequential patterns in discrete-time dynamics. Sompolinsky *et al.* have attempted to overcome this problem by assuming time delays in spin neural networks [6], and Coolen *et al.* have tried a more complicated modification of the Hebb learning rule [7]. However, as far as we know, no simple and systematic spatiotemporal learning rule has been proposed for typical neural networks without time delays.

In the present paper, we study the general spatiotemporal learning scheme that is inspired by the recent experimental findings on the spike-timing-dependent synaptic plasticity (STDP) [24–27]. Several experiments on neocortex and hippocampus pyramidal neurons have revealed that weights of some types of synapses are modified according to spike time difference between presynaptic and postsynaptic neurons; when a presynaptic neuron fires before a postsynaptic neuron, the synaptic weight is strengthened, while if the neurons fire in the opposite order, the synaptic weight is weakened. This relation of synapse modification to spike time deference is expressed by an asymmetric time window $W(\Delta t)$ as described in Fig. 1. Our aim in the present study is to incorporate this biologically plausible asymmetric time window into a learning rule so that neural networks act as spatiotemporal associative memory. In discrete-time spiking neural networks and in continuous-time spiking neural networks, the STDP-based learning rule has been shown to be effective in memorizing periodic spatiotemporal spike timings [8–10]. In the present study, we apply the STDP-based learning rule to continuous-time periodic neural activities and analyze their retrieval process in analog neural networks. We also find successful memorization of nonperiodic spatiotemporal patterns both in analog neural networks and in spiking neural networks. Based on these findings, we reveal the consider-

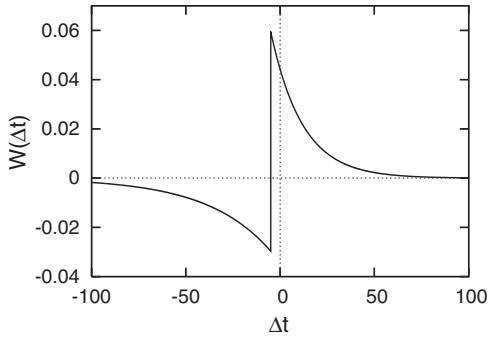

FIG. 1. The schematic shape of the time window of spike-timing-dependent synaptic plasticity (STDP) given by Eq. (50) with parameters $\tau_-=33.7$, $\tau_+=16.8$, $\tau_0=-5$, and $r=1$. The experimental studies have clarified that weights of some types of synapses are modified according to $\Delta J \propto W(\Delta t)$, where ΔJ represents change of synaptic weight and Δt denotes spike time difference between presynaptic and postsynaptic neurons.

ably wide applicability of the STDP-based learning rule to spatiotemporal learning.

Simple dynamics of analog neural networks brings various benefits to the analysis of associative memory. Thus, we adopt analog neural networks and analyze the STDP-based learning of periodic spatiotemporal patterns. Because of the assumption of periodic spatiotemporal patterns, the STDP-based learning rule is analytically reduced to a simple function of the time average of $W(\Delta t)$ and Fourier transform of $W(\Delta t)$ [11,12]. When we apply this learning rule to analog neural networks, local fields are written as summations of overlaps as in the case of the Hopfield model. Thus, provided that networks memorize a finite number of patterns, one can easily take the limit of an infinite number of neurons and obtain the dynamics of overlaps. It is interesting that this reduced learning rule is similar in style to the learning rules assumed in Potts spin neural networks and phase oscillator neural networks [13–16,28]. However, asymmetric connections given by the present learning rule make the stationary behavior of the networks more dynamical than Potts spin neural networks and phase oscillator neural networks, and that permits nonequilibrium retrieval of spatiotemporal patterns.

We find that when we encode a multiple number of patterns in the networks, the degenerate eigenvalue κ appears in linear stability analysis of the dynamics of overlaps. Evaluating this eigenvalue κ, we identify the retrieval state that is stable in single-pattern learning but unstable in multiple-pattern learning. Interestingly, this change of stability can happen even when the retrieval state is independent of a pattern number. Our analysis further shows that the storage capacity of the present associative memory is maximized when the time average of the time window $W(\Delta t)$ takes a zero value. This analytical result explains important roles of the negative and positive parts of the STDP time window in the encoding of a lot of spatiotemporal patterns.

Our analysis focuses on analog neural networks memorizing specific periodic spatiotemporal patterns. To examine the further flexibility of the STDP-based learning rule, we numerically study learning of nonperiodic spatiotemporal Poisson patterns both in analog neural networks and in spiking neural networks. In both networks, we confirm the successful retrieval of the spatiotemporal Poisson patterns.

The present paper is organized as follows. In Sec. II, we present dynamics of analog neural networks and introduce the STDP-based learning rule to encode periodic spatiotemporal patterns. In Sec. III, we derive order parameters dynamics for arbitrary form of transfer function and then analyze the stability of the retrieval state. In Sec. IV, the analysis is applied to the case when the transfer function takes the form of a Heaviside function, and then the solutions of the analysis are compared with numerical simulations. Finally, in Sec. V, we give a summary and show the results of the numerical simulations of the learning of the spatiotemporal Poisson patterns.

II. ANALOG NEURAL NETWORKS AND SPATIOTEMPORAL LEARNING BASED ON THE SPIKE-TIMING-DEPENDENT SYNAPTIC PLASTICITY

We study analog neural networks

$$\frac{d}{dt}x_i = -x_i + F(h_i), \tag{1}$$

where x_i represents the activity of neuron i, transfer function $F(h)$ denotes the input-output relationship of neurons, and local field h_i is defined by

$$h_i = \sum_j J_{ij}x_j. \tag{2}$$

In these analog neural networks we consider the problem of encoding periodic spatiotemporal patterns of the form

$$\eta_i^\mu = (1/2)[1+\cos(\omega t - \phi_i^\mu)],$$

$$i = 1, \ldots, N, \quad \mu = 1, \ldots, P, \tag{3}$$

where ω represents the frequency of periodic spatiotemporal patterns, and phase shift ϕ_i^μ is chosen randomly from the uniform distribution within the interval $[0, 2\pi)$. Spatiotemporal patterns η_i^μ are assumed to be positive valued since these patterns represent spatiotemporal firing rates. We encode these spatiotemporal patterns with a learning rule based on the spike-timing-dependent synaptic plasticity. Experimentally, synaptic modification in the STDP is expressed by $\Delta J \propto W(\Delta t)$, where ΔJ represents synapse weight change and Δt denotes spike time difference between presynaptic and postsynaptic neurons. Time window $W(\Delta t)$ takes an asymmetric shape having both negative and positive parts, as schematically shown in Fig. 1. As in our previous study [11,12], we estimate the STDP-based synapse modification for learning of a single pattern μ as

$$\Delta J_{ij}^\mu \propto \int_{-\infty}^{\infty}\int_{-\infty}^{\infty} \eta_i^\mu(t_1) W(t_1 - t_2)\, \eta_j^\mu(t_2) dt_1 dt_2. \tag{4}$$

Substituting Eq. (3) into Eq. (4), we obtain

$$\Delta J_{ij}^{\mu} \propto \int_0^{2\pi/\omega} dt_1 \int_{-\infty}^{\infty} dt_2 \frac{1}{2}[1+\cos(\omega t_1 - \phi_i^{\mu})] \times W(t_1 - t_2)\frac{1}{2}[1+\cos(\omega t_2 - \phi_j^{\mu})] \propto \mathrm{Re}(a\xi_i^{\mu}\xi_j^{\mu^*}) + 2\bar{W} \tag{5}$$

with

$$\xi_i^{\mu} = e^{i\phi_i^{\mu}}, \tag{6}$$

where asterisk indicates complex conjugate, and complex number a and real number $\bar{W}$ are defined by

$$a = \int_{-\infty}^{\infty} W(t)e^{-i\omega t}dt \tag{7}$$

and

$$\bar{W} = \int_{-\infty}^{\infty} W(t)dt. \tag{8}$$

It is worthy to note that variable a is a Fourier component of time window $W(\Delta t)$ corresponding to pattern frequency ω and $\bar{W}$ is the time average of time window $W(\Delta t)$. We extend this single pattern learning rule to the case of multiple patterns η_i^{μ} $(\mu=1,2,\ldots,P)$. Applying the proper scaling, we obtain the following learning rule:

$$J_{ij} = \frac{1}{N}\sum_{\mu=1}^{P} \mathrm{Re}(a\xi_i^{\mu}\xi_j^{\mu^*}) + \frac{b}{N} \tag{9}$$

with

$$b = 2P\bar{W}. \tag{10}$$

This is the learning rule we study in the what follows. We generate random spatiotemporal patterns (3) and determine synapse connections by the learning rule (9). Then, with these quenched synapse connections, we conduct numerical simulations and theoretical analysis. Note that both in numerical simulations and in analysis, synapse connections are fixed over time.

The result of the numerical simulation in Fig. 2 illustrates how learning rule (9) contributes to spatiotemporal learning in analog neural networks. In this numerical simulation, we randomly generate three spatiotemporal patterns η_i^{μ} $(\mu=1,2,3)$. Figure 2(a) describes the first spatiotemporal pattern η_i^1. We encode these three spatiotemporal patterns by learning rule (9), and then carry out the numerical integration of the dynamics of analog neural networks with the Heaviside function (48) under the initial condition $x_i(0)=\eta_i^1(0)$. The behavior of analog neurons in this numerical simulation is described in Fig. 2(b). Note that while the wave forms of x_i in Fig. 2(b) are different from those of η_i^1 in Fig. 2(a), the phase shifts ϕ_i^1 in Fig. 2(a) are well reproduced in the spatiotemporal pattern in Fig. 2(b). In this sense, initial condition $x_i(0)=\eta_i^1(0)$ leads to retrieval of pattern $\eta_i^1(t)$, preserving the phase relation among components $\eta_i^1(t)$ and changing the oscillation frequency to the faster one [note that the X-axis scale of Fig. 2(a) is different than that of Fig. 2(b)].

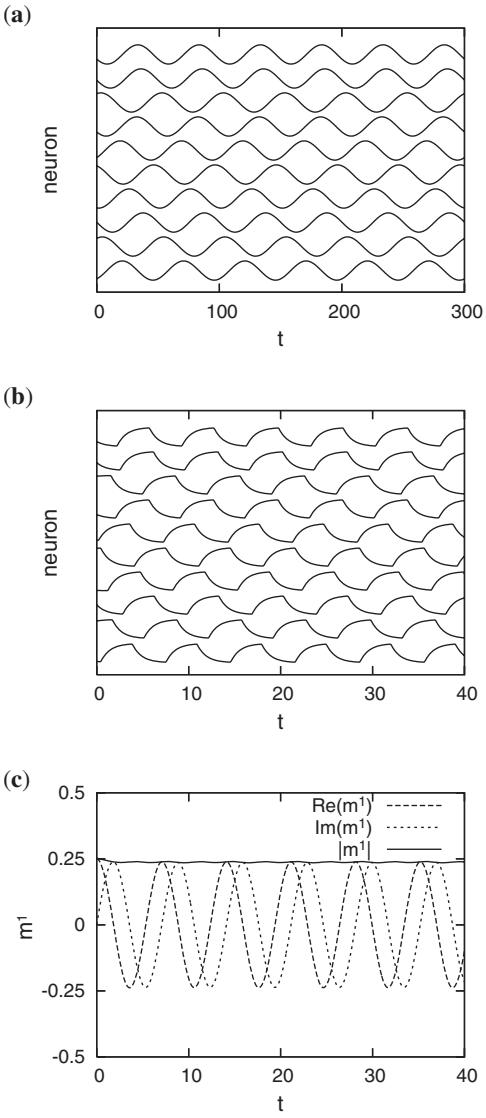

FIG. 2. The result of the numerical simulation of associative memory of analog neural networks with the STDP-based learning rule. In this numerical simulation, three periodic spatiotemporal patterns η_i^{μ} $(\mu=1,\ldots,3)$ are generated randomly at frequency $\omega=0.02\times 2\pi$, and then encoded in networks of 10 000 analog neurons according to the learning rule (7)–(10) by using the time window $W(\Delta t)$ in Fig. 1(a). The first pattern η_i^1 is plotted as a function of time only for the first ten neurons $(i=1,\ldots,10)$. (b) The behavior of first ten neurons x_i in the numerical simulation are plotted as a function of time. The analog neuron dynamics (1) is computed with the Heaviside function (48). The initial condition is set to $x_i(0)=\eta_i^1(0)$, which induces the retrieval of pattern 1. (c) The time evolution of overlap m^1 defined by Eq. (11) is plotted as a function of time.

To measure the similarity of x_i to encoded phase shift ϕ_i^1, we define overlaps for pattern μ as

$$m^{\mu} = \frac{1}{N}\sum_{i} \xi_i^{\mu} x_i. \tag{11}$$

The time evolution of overlap m^1 is described in Fig. 2(c). Owing to periodic behavior of x_i, complex number m^1 exhibits its periodic oscillation on complex plain. After a long time, overlap m^1 settles into the stationary state with constant absolute value and constant angular frequency, reflecting the successful retrieval of the first pattern. In the following we represent this retrieval frequency of the overlap by $\tilde{\omega}$. Retrieval frequency $\tilde{\omega}$ takes a different value from pattern frequency ω since retrieval occurs at a time scale different from encoded patterns. Also note that while overlap m^1 shows periodic oscillation with a nonzero amplitude, other overlaps (i.e., m^2 and m^3) remain close to zero (data not shown).

III. ANALYSIS OF ANALOG NEURAL NETWORKS WITH LEARNING RULE (9)

To investigate the above-mentioned time evolution of overlaps, we derive dynamics of order parameters for the present analog neural networks. Note that in the present section we analyze neural networks with learning rule (9). In fact, variables a and b in learning rule (9) are determined through Eqs. (7), (8), and (10), and hence functions of various learning parameters, such as pattern frequency ω, number of patterns P, and the shape of time window $W(\Delta t)$. Nevertheless, during the present section, we treat variables a and b just as certain constant parameters. In the later sections, such as Secs. IV A and IV B, we substitute Eqs. (7), (8), and (10) into variables a and b, and discuss the influence of the above-mentioned learning parameters on retrieval properties. Also note that pattern number P is assumed to be finite throughout the paper. For finite P, we take the limit of an infinite number of neurons ($N \to \infty$) to obtain dynamics of order parameters.

A. Dynamics of order parameters

We define mean activity X by

$$X = \frac{1}{N}\sum_{i} x_i. \tag{12}$$

Then, from Eqs. (9), (11), and (12), we rewrite local field (2) in the form

$$h_i = \sum_{\mu} \mathrm{Re}(a\xi_i^{\mu} m^{\mu *}) + bX. \tag{13}$$

Therefore, from Eqs. (1) and (11), we obtain dynamics of overlaps

$$\begin{aligned} \frac{d}{dt}m^{\mu} &= -m^{\mu} + \frac{1}{N}\sum_{i} \xi_i^{\mu} F\left(\sum_{\nu} \mathrm{Re}(a\xi_i^{\nu} m^{\nu *}) + bX\right) \\ &= -m^{\mu} + \left\langle \xi^{\mu} F\left(\sum_{\nu} \mathrm{Re}(a\xi^{\nu} m^{\nu *}) + bX\right)\right\rangle, \end{aligned} \tag{14}$$

where we take the limit $N \to \infty$ for finite P to replace the summation over i by the average $\langle \cdots \rangle$ defined by

$$\begin{aligned} \frac{1}{N}\sum_{i} f(\xi_i^1, \xi_i^2, \ldots, \xi_i^P) &= \langle f(\xi^1, \xi^2, \ldots, \xi^P)\rangle \\ &= \frac{1}{(2\pi)^P}\int_0^{2\pi} d\phi^1 \int_0^{2\pi} d\phi^2 \cdots \int_0^{2\pi} d\phi^P \\ &\quad \times f(e^{i\phi^1}, e^{i\phi^2}, \ldots, e^{i\phi^P}). \end{aligned} \tag{15}$$

In the same manner, from Eqs. (1) and (12), we obtain the dynamics of X as

$$\frac{d}{dt}X = -X + \left\langle F\left(\sum_{\nu} \mathrm{Re}(a\xi^{\nu} m^{\nu *}) + bX\right)\right\rangle. \tag{16}$$

Equations (14) and (16) yield the closed dynamics for overlap $m^{\mu}(\mu = 1, \ldots, P)$ and mean activity X. Since complex number m^{μ} is effectively two dimensional, the total dimension of dynamics (14) and (16) is $2P+1$. Order parameter dynamics (14) and (16) thus enables one to carry out a much more efficient investigation than the original N-dimensional neural networks.

We can reduce $(2P+1)$-dimensional dynamics (14) and (16) further by representing the overlap in the polar form

$$m^{\mu} = |m^{\mu}| e^{i\theta^{\mu}}. \tag{17}$$

Substitution of Eq. (17) into Eq. (14) yields

$$\begin{aligned} \frac{d|m^{\mu}|}{dt} e^{i\theta^{\mu}} + |m^{\mu}| e^{i\theta^{\mu}}\left(i\frac{d\theta^{\mu}}{dt}\right) &= -|m^{\mu}| e^{i\theta^{\mu}} + \left\langle \xi^{\mu} F\left(\sum_{\nu} \mathrm{Re}(a\xi^{\nu}|m^{\nu}| e^{-i\theta^{\nu}}) + bX\right)\right\rangle \\ &= -|m^{\mu}| e^{i\theta^{\mu}} + \frac{1}{(2\pi)^P}\int \prod_{\nu'=1}^{P} d\phi^{\nu'} e^{i\phi^{\mu}} F\left(\sum_{\nu} \mathrm{Re}(a|m^{\nu}| e^{i(\phi^{\nu} - \theta^{\nu})}) + bX\right) \\ &= -|m^{\mu}| e^{i\theta^{\mu}} + e^{i\theta^{\mu}}\frac{1}{(2\pi)^P}\int \prod_{\nu'=1}^{P} d\phi^{\nu'} e^{i\phi^{\mu}} F\left(\sum_{\nu} \mathrm{Re}(a|m^{\nu}| e^{i\phi^{\nu}}) + bX\right) \\ &= -|m^{\mu}| e^{i\theta^{\mu}} + e^{i\theta^{\mu}}\left\langle \xi^{\mu} F\left(\sum_{\nu} \mathrm{Re}(a\xi^{\nu}|m^{\nu}|) + bX\right)\right\rangle. \end{aligned} \tag{18}$$

Therefore, we obtain

$$\frac{d}{dt}|m^\mu| = -|m^\mu| + \left\langle \mathrm{Re}(\xi^\mu) F\left(\sum_\nu \mathrm{Re}(a\xi^\nu |m^\nu|) + bX \right) \right\rangle \tag{19}$$

and

$$\frac{d}{dt}\theta^\mu = \frac{1}{|m^\mu|} \left\langle \mathrm{Im}(\xi^\mu) F\left(\sum_\nu \mathrm{Re}(a\xi^\nu |m^\nu|) + bX \right) \right\rangle. \tag{20}$$

Equation (19) describes the dynamics of absolute value of overlap m^μ, while $d\theta^\mu/dt$ in Eq. (20) gives the frequency of oscillation of overlap m^μ. Following the similar scheme, we rewrite Eq. (16) in the form

$$\frac{d}{dt}X = -X + \left\langle F\left(\sum_\nu \mathrm{Re}(a\xi^\nu |m^\nu|) + bX \right) \right\rangle. \tag{21}$$

Equations (19) and (21) yield $(P+1)$-dimensional closed dynamics for $|m^\mu|$ $(\mu=1,\ldots,P)$ and X, that is, we can analyze the behavior of $|m^\mu|$ $(\mu=1,\ldots,P)$ and X without calculating Eq. (20). Note, however, that determination of oscillation frequency of overlaps requires evaluation of Eq. (20).

B. Retrieval state

To investigate the properties of retrieval state, we analyze fixed points of dynamics (19) and (21). In the successful pattern retrieval described in Fig. 2, overlap m^1 eventually settles into the stationary state with the constant absolute value, while other overlaps m^μ $(\mu=2,\ldots,P)$ remain close to zero. We mathematically define this retrieval state as

$$|m^1| \neq 0, \tag{22}$$

$$|m^2| = |m^3| = \cdots = |m^P| = 0, \tag{23}$$

and

$$\frac{d}{dt}|m^1| = \frac{d}{dt}X = 0, \tag{24}$$

where we safely assume m^1 as a retrieved pattern.

We substitute Eqs. (22)–(24) into Eq. (19) and obtain

$$\begin{aligned} |m^1| &= \langle \mathrm{Re}(\xi^1) F[\mathrm{Re}(a\xi^1 |m^1|) + bX] \rangle \\ &= \frac{1}{2\pi} \int_0^{2\pi} \cos\phi^1 F[|a||m^1|\cos(\phi^1+\varphi) + bX] d\phi^1, \end{aligned} \tag{25}$$

where variable φ is defined by the polar form of variable a

$$a = |a| e^{i\varphi}. \tag{26}$$

Applying the same scheme to Eq. (21), we have

$$\begin{aligned} X &= \langle F[\mathrm{Re}(a\xi^1 |m^1|) + bX] \rangle \\ &= \frac{1}{2\pi} \int_0^{2\pi} F[|a||m^1|\cos(\phi^1+\varphi) + bX] d\phi^1. \end{aligned} \tag{27}$$

A solution of Eqs. (25) and (27) determines $|m^1|$ and X in retrieval state. These equations can be solved numerically for arbitrary form of transfer function $F(h)$.

Retrieval frequency $\tilde{\omega}$, namely, oscillation frequency of an overlap in retrieval state, is given as

$$\tilde{\omega} = \frac{d\theta^1}{dt}, \tag{28}$$

where $d\theta^1/dt$ represents the time derivative of θ^1 in retrieval state. Therefore, we substitute Eqs. (22)–(24) into Eq. (20), and obtain

$$\begin{aligned} \tilde{\omega} &= \frac{1}{|m^1|} \langle \mathrm{Im}(\xi^1) F[\mathrm{Re}(a\xi^1 |m^1|) + bX] \rangle \\ &= \frac{1}{2\pi |m^1|} \int_0^{2\pi} \sin\phi^1 F[|a||m^1|\cos(\phi^1+\varphi) + bX] d\phi^1 \\ &= -\frac{\sin\varphi}{\pi |m^1|} \int_0^{\pi} \cos\phi^1 F(|a||m^1|\cos\phi^1 + bX) d\phi^1. \end{aligned} \tag{29}$$

In the last line of the above calculations, we simplify the integral by changing variable ϕ^1 by $\phi^1-\varphi$. Applying the same simplification to Eq. (25), we obtain

$$|m^1| = \frac{\cos\varphi}{\pi} \int_0^{\pi} \cos\phi^1 F(|a||m^1|\cos\phi^1 + bX) d\phi^1. \tag{30}$$

Substitution Eq. (30) into Eq. (29) yields

$$\tilde{\omega} = -\tan\varphi. \tag{31}$$

This implies that retrieval frequency $\tilde{\omega}$ is determined only by φ, namely, the phase of the Fourier component of time window $W(\Delta t)$ corresponding to pattern frequency ω.

C. Stability of retrieval state in networks with a single encoded pattern ($P=1$)

The solution of Eqs. (25) and (27) yields fixed points of the dynamics (19) and (21). However, some of these solutions are unstable fixed points, which are useless for the purpose of associative memories. In this section, we analyze linear stability of solutions of Eqs. (25) and (27), assuming that only a single pattern is encoded in networks $(P=1)$. We discuss the case of multiple patterns $(1<P)$ in the next section.

To evaluate linear stability of the solutions, we consider perturbed state $|m^1|+\delta|m^1|$ and $X+\delta X$, where $|m^1|$ and X represent a solution of Eqs. (25) and (27). From Eqs. (19) and (25), dynamics of $\delta|m^1|$ is given as

$$\begin{aligned} \frac{d}{dt}\delta|m^1| &= -\delta|m^1| + \langle \mathrm{Re}(\xi^1) F'[\mathrm{Re}(a\xi^1|m^1|) + bX] \\ &\quad \times [\mathrm{Re}(a\xi^1)\delta|m^1| + b\delta X] \rangle \\ &= -\delta|m^1| + I(\xi^1, a\xi^1)\delta|m^1| + I(\xi^1, b)\delta X, \end{aligned} \tag{32}$$

where we use an abbreviation

$$I(f,g) = \langle \mathrm{Re}(f) F'[\mathrm{Re}(a\xi^1|m^1|) + bX] \mathrm{Re}(g) \rangle. \tag{33}$$

From Eqs. (21) and (27), dynamics of δX is obtained as

$$\frac{d}{dt}\delta X = -\delta X + \langle F'[\mathrm{Re}(a\xi^1|m^1|) + bX][\mathrm{Re}(a\xi^1)\delta|m^1| + b\delta X]\rangle$$
$$= -\delta X + I(1,a\xi^1)\delta|m^1| + I(1,b)\delta X. \quad (34)$$

We can summarize Eqs. (32) and (34) in the form

$$\frac{d}{dt}\begin{pmatrix}\delta X\\ \delta|m^1|\end{pmatrix} = \mathbf{A}\begin{pmatrix}\delta X\\ \delta|m^1|\end{pmatrix} \quad (35)$$

with

$$\mathbf{A} = \begin{pmatrix}-1 + I(1,b) & I(1,a\xi^1)\\ I(\xi^1,b) & -1 + I(\xi^1,a\xi^1)\end{pmatrix}. \quad (36)$$

We represent eigenvalues of matrix $\mathbf{A}$ by λ_1 and λ_2. A solution of Eqs. (25) and (27) is stable if eigenvalues λ_1 and λ_2 satisfy the condition

$$\mathrm{Re}(\lambda_l) < 0,\ l = 1,2. \quad (37)$$

D. Stability of retrieval state in networks with multiple encoded patterns ($1 < P$)

When multiple patterns are encoded ($1 < P$), we have to analyze perturbations of nonretrieved patterns $\delta|m^\mu|$ ($\mu = 2,\ldots,P$) as well as $\delta|m^1|$ and δX. Following the same scheme as Eqs. (32) and (34), we obtain dynamics of $\delta|m^\mu|$ ($\mu = 1,\ldots,P$) as

$$\frac{d}{dt}\delta|m^\mu| = -\delta|m^\mu| + \left\langle \mathrm{Re}(\xi^\mu)F'[\mathrm{Re}(a\xi^1|m^1|) + bX] \times\left[\sum_\nu \mathrm{Re}(a\xi^\nu)\delta|m^\nu| + b\delta X\right]\right\rangle$$
$$= -\delta|m^\mu| + \sum_\nu I(\xi^\mu,a\xi^\nu)\delta|m^\nu| + I(\xi^\mu,b)\delta X, \quad (38)$$

and dynamics of δX as

$$\frac{d}{dt}\delta X = -\delta X + \left\langle F'[\mathrm{Re}(a\xi^1|m^1|) + bX] \times\left[\sum_\nu \mathrm{Re}(a\xi^\nu)\delta|m^\nu| + b\delta X\right]\right\rangle$$
$$= -\delta X + \sum_\nu I(1,a\xi^\nu)\delta|m^\nu| + I(1,b)\delta X. \quad (39)$$

Equations (38) and (39) are summarized as

$$\frac{d}{dt}\begin{pmatrix}\delta X\\ \delta|m^1|\\ \delta|m^2|\\ \vdots\\ \delta|m^P|\end{pmatrix} = \mathbf{B}\begin{pmatrix}\delta X\\ \delta|m^1|\\ \delta|m^2|\\ \vdots\\ \delta|m^P|\end{pmatrix} \quad (40)$$

with

$$\mathbf{B} = \begin{pmatrix}-1 + I(1,b) & I(1,a\xi^1) & I(1,a\xi^2) & \cdots & I(1,a\xi^P)\\ I(\xi^1,b) & -1 + I(\xi^1,a\xi^1) & I(\xi^1,a\xi^2) & \cdots & I(\xi^1,a\xi^P)\\ I(\xi^2,b) & I(\xi^2,a\xi^1) & -1 + I(\xi^2,a\xi^2) & \cdots & I(\xi^2,a\xi^P)\\ \vdots & \vdots & \vdots & \ddots & \vdots\\ I(\xi^P,b) & I(\xi^P,a\xi^1) & I(\xi^P,a\xi^2) & \cdots & -1 + I(\xi^P,a\xi^P)\end{pmatrix}. \quad (41)$$

From the definition of $I(f,g)$ in Eq. (33), it is straightforward to show

$$I(1,a\xi^\mu) = I(\xi^1,a\xi^\mu) = I(\xi^\mu,b) = I(\xi^\mu,a\xi^1) = 0,$$
$$2 \leqslant \mu, \quad (42)$$

and

$$I(\xi^\mu,a\xi^\nu) = 0, \quad 2 \leqslant \mu,\nu,\mu \neq \nu. \quad (43)$$

These relations imply that a lot elements in matrix $\mathbf{B}$ take the zero values. Noting the further relations

$$I(\xi^\mu,a\xi^\mu) = I(\xi^2,a\xi^2), \quad 2 \leqslant \mu, \quad (44)$$

we can rewrite matrix $\mathbf{B}$ in the form

$$\mathbf{B} = \begin{pmatrix}\mathbf{A} & & & \mathbf{0}\\ & -1 + I(\xi^2,a\xi^2) & & \\ & & \ddots & \\ \mathbf{0} & & & -1 + I(\xi^2,a\xi^2)\end{pmatrix}, \quad (45)$$

where $\mathbf{A}$ represents the matrix defined by Eq. (36). Therefore, matrix $\mathbf{B}$ has the same eigenvalues as matrix $\mathbf{A}$ (i.e., λ_1 and λ_2), and degenerate eigenvalue

$$\kappa = -1 + I(\xi^2,a\xi^2). \quad (46)$$

A solution of Eqs. (25) and (27) is stable when the eigenvalues satisfy the condition

$$\mathrm{Re}(\lambda_l) < 0 \text{ and } \mathrm{Re}(\kappa) < 0,\ l = 1,2. \quad (47)$$

While stability of solutions with a single encoded pattern ($P = 1$) is determined only from λ_1 and λ_2, stability with mul-

tiple encoded patterns $(1<P)$ requires further evaluation of eigenvalue κ. As will be shown in the next section, under a certain condition, $\mathrm{Re}(\kappa)$ takes a positive value while $\mathrm{Re}(\lambda_1)$ and $\mathrm{Re}(\lambda_2)$ take negative values. In such a case, stable retrieval state with a single pattern $(P=1)$ becomes unstable with multiple patterns $(1<P)$. Evaluation of κ is thus indispensable for analyzing the phase transition occurring with multiple encoded patterns $(1<P)$ even when the solution with multiple patterns $(1<P)$ is the same as a single pattern $(P=1)$.

IV. THE CASE OF THE HEAVISIDE FUNCTION

Let us apply the above analysis to the case when transfer function $F(h)$ is represented by the Heaviside function of the form

$$F(h) = H(h) = \begin{cases} 0, & h < 0, \\ 1, & 0 \leq h. \end{cases} \tag{48}$$

Assuming this Heaviside function, we aim to investigate how positive-valued spatiotemporal patterns η_i^μ are retrieved in analog neural networks with positive-valued transfer function. As shown in the Appendix, the assumption of the Heaviside function simplifies the calculation of the quantities $|m^1|$ and X, and of eigenvalues λ_1, λ_2, and κ. Because of the simple relation

$$H(h_i) = H\left(\sum_j \left\{ \frac{1}{N} \sum_\mu \mathrm{Re}(a \xi_i^\mu \xi_j^{\mu *}) + \frac{b}{N} \right\} x_j \right)$$
$$= H\left(\sum_j \left\{ \frac{1}{N} \sum_\mu \mathrm{Re}(e^{i\varphi} \xi_i^\mu \xi_j^{\mu *}) + \frac{b/|a|}{N} \right\} x_j \right), \tag{49}$$

all analytical results in the Appendix take the form of functions of $b/|a|$. Therefore, we treat $b/|a|$ almost as an independent parameter in the present section.

Typical behavior of overlap m^1 and eigenvalues λ_1, λ_2, and κ are plotted as functions of $b/|a|$ in Fig. 3. Within the interval $0<b/|a|<0.15$, Eqs. (19) and (21) have two solutions, which are described by thick and dotted lines in Fig. 3(a). When a single pattern is encoded, eigenvalues λ_1 and λ_2 determine stability of solutions. Equation (A13) shows that λ_1 always takes the value of -1. Meanwhile, as described in Fig. 3(b), $\mathrm{Re}(\lambda_2)$ takes a negative value for the solution with the thick line and a positive value for the solution with the dotted line. This implies that the thick line in Fig. 3(a) represents the stable retrieval state, while the dotted line represents the unstable retrieval state.

When we encode multiple patterns $(1<P)$, we have to evaluate eigenvalue κ as well as eigenvalues λ_1 and λ_2. We draw the vertical dotted line in all three figures in Fig. 3 so as to indicate the critical point $(b/|a|)^c \sim -0.45$, at which $\mathrm{Re}(\kappa)$ takes the zero value as shown in Fig. 3(c). Beyond the vertical line [i.e., $(b/|a|)^c < b/|a|$], the retrieval state with the thick line in Fig. 3(a) is always stable since $\mathrm{Re}(\kappa)$ is negative. However, below the vertical dotted line [i.e., $b/|a| < (b/|a|)^c$], $\mathrm{Re}(\kappa)$ is positive, and the retrieval state with the thick line becomes unstable. Positive $\mathrm{Re}(\kappa)$ below the vertical dotted line thus induces phase transition, in which stable retrieval state with a single encoded pattern $(P=1)$ becomes unstable with multiple patterns $(1<P)$.

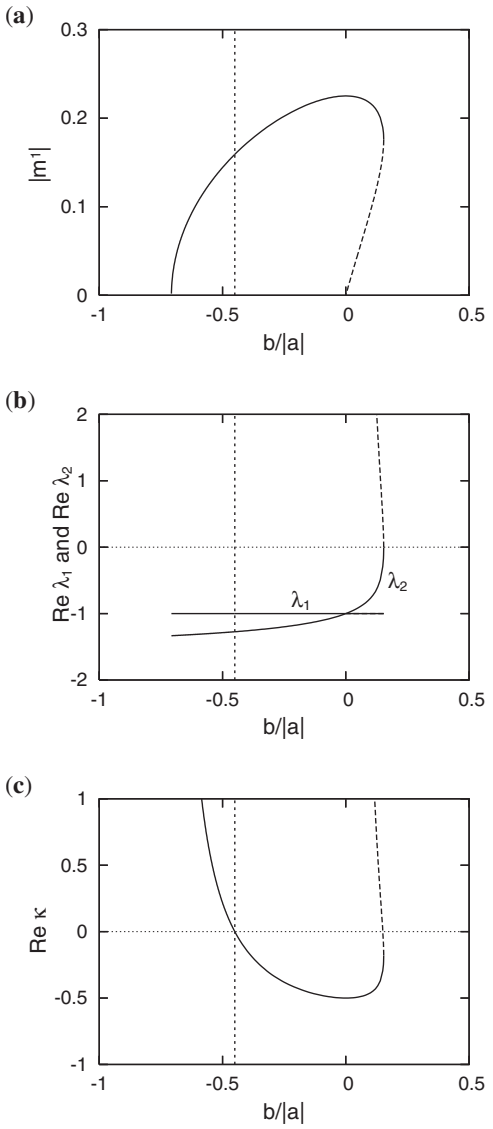

FIG. 3. (a) A fixed point of dynamics (19) and (21) with the Heaviside function (48) is plotted as a function of $b/|a|$ for $\varphi = -\pi/4$. The thick line and the dotted line are utilized to distinguish multiple solutions arising in the interval $0<b/|a|<0.15$. (b) Real parts of eigenvalues λ_1 and λ_2 of matrix **A** are plotted. Eigenvalue λ_1 takes -1 for both the solutions (i.e., the thick line and the dotted line). Meanwhile, eigenvalue λ_2 takes different values for different solutions, which are indicated by the thick line and the dotted line in the same way as (a). (c) The real part of eigenvalue κ of matrix **B** is plotted. The thick line and the dotted line corresponds to the two different solutions described in (a). The vertical dotted line are plotted in all three figures so as to indicate the critical point $(b/|a|)^c \sim -0.45$, at which $\mathrm{Re}(\kappa)$ takes the zero value.

The numerical simulations in Figs. 4–6 illustrate the phase transition induced by eigenvalue κ. In Fig. 4, we set $a=1$ and $b=-0.4$, with which $b/|a|$ is beyond the critical point $(b/|a|)^c$. Therefore, overlap $|m^1|$ in Fig. 4 shows successful pattern retrieval even when we encode multiple pat-

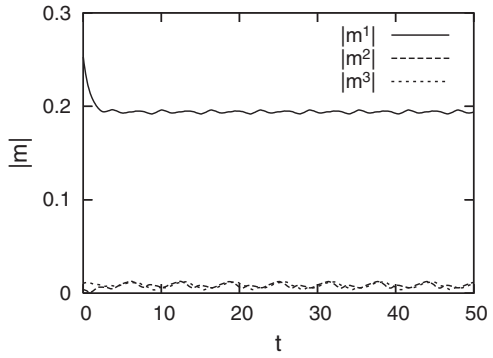

FIG. 4. The numerical simulation of analog neural networks with the Heaviside function is carried out for $N=10\,000$, $P=3$, $\varphi=-\pi/4$, $|a|=1$, and $b=-0.4$. Absolute values of all overlaps are plotted as a function of time.

terns $P=3$. Figure 5 describes the results of the numerical simulations with $a=1$ and $b=-0.6$, with which $b/|a|$ is below the critical point. As shown in Fig. 5(a), retrieval is successful when a single pattern is encoded ($P=1$). However, when we encode multiple patterns as in the cases of Figs. 5(b) ($P=2$) and 5(c) ($P=3$), retrieval is impossible since nonretrieved overlaps $m^{\mu}(\mu \neq 1)$ increase their size as a result of positive $\mathrm{Re}(\kappa)$. In Figs. 5(b) and 5(c), the network seems to settle into mixture state.

In Fig. 6, we compare the sizes of overlaps in numerical simulations with theoretical values. As shown in Fig. 6(a), the numerical simulations with $P=1$ show a good agreement with the thick line for all the value of $b/|a|$. On the other hand, the numerical simulations in Fig. 6(b) ($P=2$) and 6(c) ($P=3$) deviate from the thick line below the vertical dotted line as a result of positive $\mathrm{Re}(\kappa)$. These numerical simulations clearly indicate the occurrence of the phase transition at $(b/|a|)^c$.

Figure 7(a) shows the φ-$(b/|a|)$ phase diagram drawn from our analysis. Retrieval state with negative $\mathrm{Re}(\lambda_1)$ and $\mathrm{Re}(\lambda_2)$ is found inside the region enclosed by thick line. In the region with "$P \geqslant 1$," $\mathrm{Re}(\kappa)$ takes a negative value, and retrieval state is always stable for arbitrary finite value of P. However, in the region denoted by "$P=1$," retrieval is possible only with $P=1$ since $\mathrm{Re}(\kappa)$ takes a positive value. Figure 7(b) shows retrieval frequency $\tilde{\omega}$. Note that retrieval frequency $\tilde{\omega}$ is a function of φ as shown in Eq. (31), and does not depend on other parameters such as variables $|a|$ and b. With negative φ, frequency $\tilde{\omega}$ takes a positive value, and the overlap oscillates to the same direction as encoded pattern. Oscillation becomes considerably fast near $\varphi=-\pi/2$ since $\tilde{\omega}$ diverges at $\varphi=-\pi/2$. Frequency $\tilde{\omega}$ decreases as φ increases, and oscillation stops at $\varphi=0$. When φ is positive, frequency $\tilde{\omega}$ takes a negative value, and the overlap oscillates to the direction opposite to the encode patterns. In this case, networks retrieve encoded patterns in the reversed order with respect to time.

A. The relation of retrieval state to the STDP time window

The above analysis has clarified the role of learning rule (9) in associative memory of analog neural networks. We

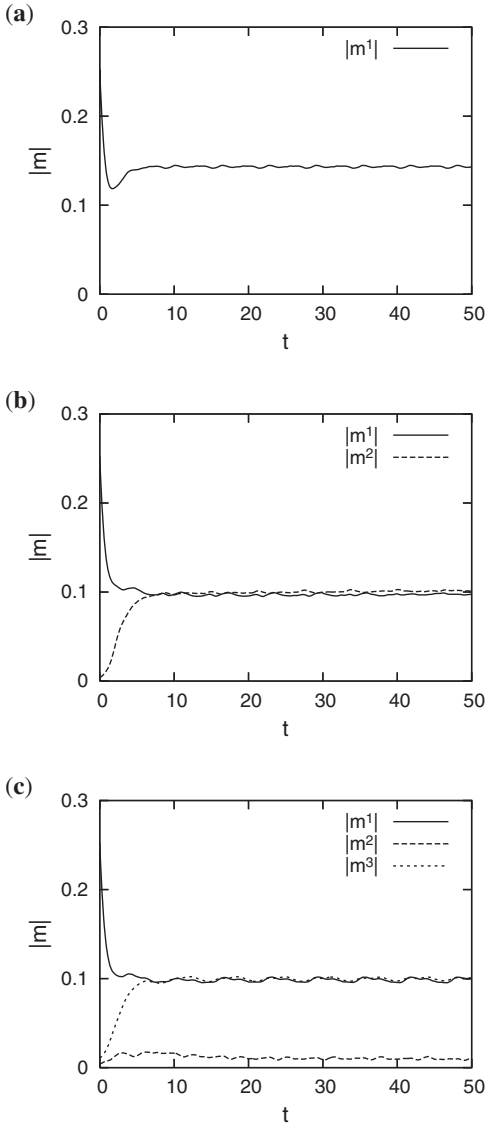

FIG. 5. The numerical simulations of analog neural networks with the Heaviside function are carried out for $N=10\,000$, $\varphi=-\pi/4$, $|a|=1$, and $b=-0.6$ with the pattern number (a) $P=1$, (b) $P=2$, and (c) $P=3$. Absolute values of all overlaps are plotted as a function of time. The high absolute value of the overlap in (a) ($|m^1| \sim 0.14$) indicates the successful pattern retrieval, while the low absolute value of the overlap in (b) and (c) ($|m^1| \sim 0.1$) implies settlement to mixture state.

now substitute Eqs. (7), (8), and (10) into variables a and b, and investigate the influence of the STDP time window on the retrieval properties of analog neural networks.

We focus on the STDP time window of the form

$$W(\Delta t) = \begin{cases} -\dfrac{r}{\tau_-} e^{(\Delta t - \tau_0)/\tau_-} & \Delta t \leqslant \tau_0, \\ \dfrac{1}{\tau_+} e^{-(\Delta t - \tau_0)/\tau_+} & \tau_0 < \Delta t, \end{cases} \tag{50}$$

where parameters τ_- and τ_+ represent decay time of STDP time window and parameter τ_0 denotes time shift. Parameter r controls the size of a negative part of the time window

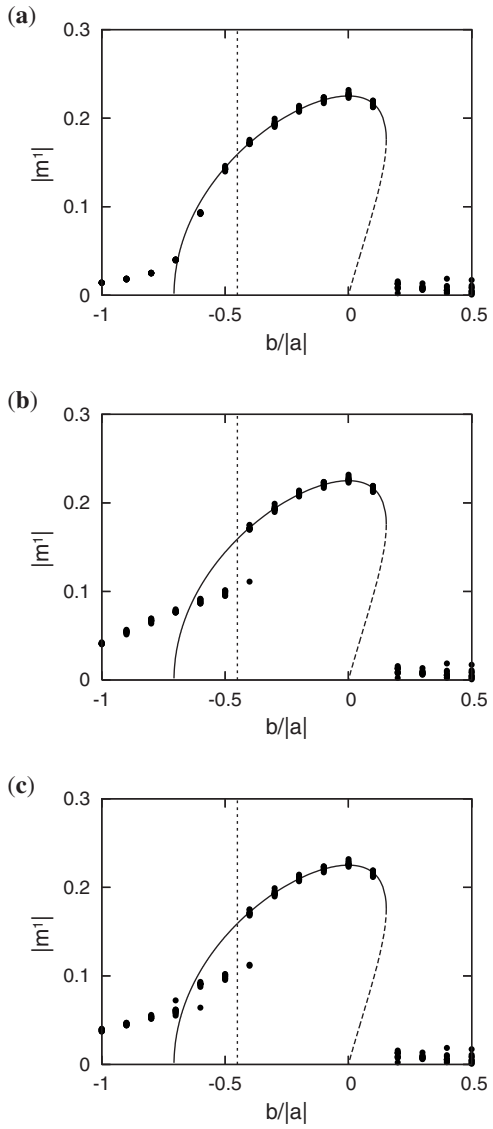

FIG. 6. The comparisons of the numerical simulations and the analytical results. Changing the value of b, we carry out several numerical simulations for (a) $P=1$, (b) $P=2$, and (c) $P=3$. Ten numerical simulations are conducted for each value of b, and absolute values of stationary overlaps are plotted. The curved line and the vertical line represent the analytical results shown in Fig. 3. The numerical simulations are carried out with the parameters $N=10\,000$, $\varphi=-\pi/4$, and $|a|=1$.

$W(\Delta t)$; when r takes one, the area of the negative part is equal to the area of the positive part. Figure 1 shows the example of STDP time window defined by Eq. (50). In the present section, the parameter values of the time window is set to be the same as Fig. 1, except for $r=1.125$.

Substitution of Eq. (50) into Eq. (7) yields

$$a = e^{-i\omega\tau_0}\left(\frac{1}{1+i\omega\tau_+} - \frac{r}{1-i\omega\tau_-}\right). \tag{51}$$

The time average of the time window $\bar{W}$ in Eq. (8) is given as $\bar{W}=1-r$. Therefore, from Eq. (10), we obtain

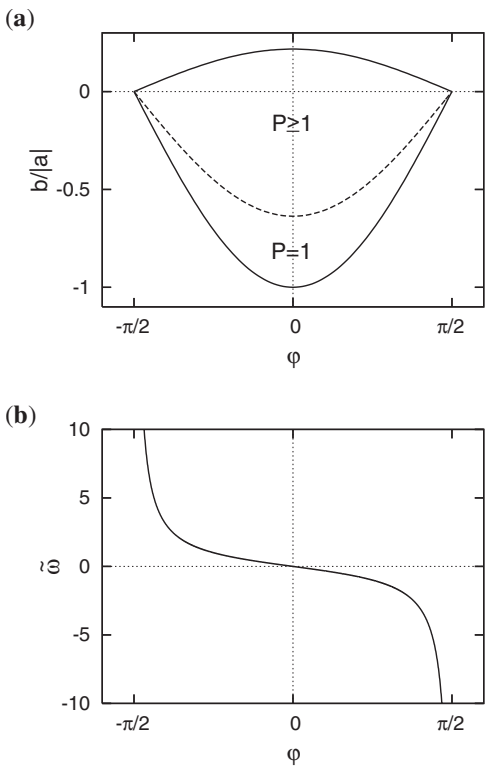

FIG. 7. (a) $\varphi-(b/|a|)$ phase diagram for analog neural networks with the Heaviside function. Retrieval state with negative $\mathrm{Re}(\lambda_1)$ and $\mathrm{Re}(\lambda_2)$ is found in the region enclose by the thick line. In the region with "$P=1$," $\mathrm{Re}(\kappa)$ takes a positive value, and retrieval state is stable only when we encode a single pattern ($P=1$). Meanwhile, in the region with "$P\geqslant 1$," $\mathrm{Re}(\kappa)$ takes a negative value, and retrieval state is stable for arbitrary finite value of P. (b) From Eq. (31), we calculate retrieval frequency $\tilde{\omega}$ as a function of φ. Note that this retrieval frequency $\tilde{\omega}$ is only valid for stable retrieval state in $\varphi-(b/|a|)$ phase diagram.

$$b = 2P(1-r). \tag{52}$$

Equation (51) indicates that variable a is a function of pattern frequency ω. Therefore, with change of pattern frequency ω, point $(b/|a|,\varphi)$ moves on the $\varphi-(b/|a|)$ phase diagram as shown in Fig. 8(a), where we draw the trajectories for $P=1$ and $P=2$. With $\omega=0$ and $P=1$, point $(b/|a|,\varphi)$ locates at $(-2P,-\pi)$. As ω increases, point $(b/|a|,\varphi)$ proceeds to the direction indicated by the arrow. With $P=1$, the trajectory has an intersection with the retrieval phase denoted by "$P=1$" and "$P\geqslant 1$," at which networks can retrieve patterns. Retrieval frequency $\tilde{\omega}$ at this intersection is plotted as a function of ω in Fig. 8(b). Interestingly, as ω increases, oscillation frequency $\tilde{\omega}$ decreases, and even takes a negative value beyond $\omega\sim 0.30$.

On the other hand, when we encode multiple patterns ($1<P$), networks cannot retrieve patterns since the trajectory with $P=2$ in Fig. 8 has no intersection with the retrieval phase denoted by "$P\geqslant 1$." Although this trajectory with $P=2$ has a small intersection with the phase denoted by "$P=1$," the phase denoted by "$P=1$" is useless for the case of $P=2$. Since variable b in Eq. (52) is proportional to P, the

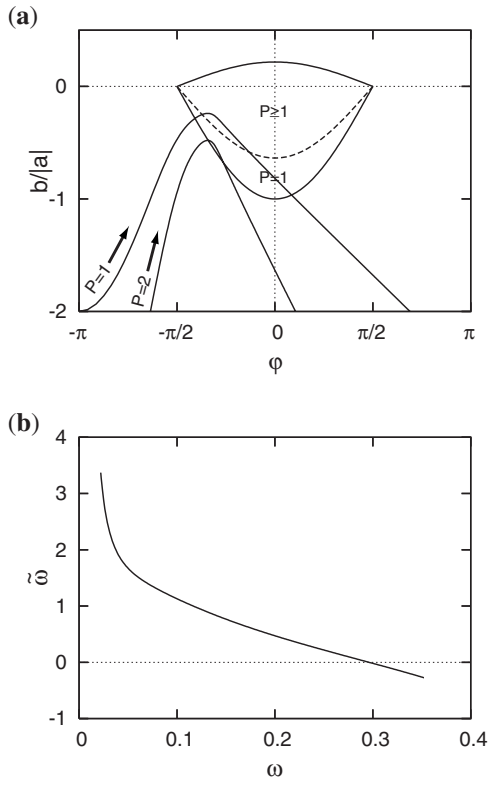

FIG. 8. (a) The trajectory of $(\varphi, b/|a|)$ calculated from Eqs. (51) and (52) with change of ω is plotted on $\varphi-(b/|a|)$ phase diagram for $P=1$ and $P=2$. As ω increases, point $(\varphi, b/|a|)$ proceeds in the direction indicated by the arrow. (b) The retrieval frequency of overlap $\tilde{\omega}$ is plotted as a function of ω for $P=1$. With $P=2$, retrieval is impossible since the trajectory with $P=2$ has no intersection with the retrieval region with "$P \geqslant 1$." The parameters for the time window are set to be the same as Fig. 1 except for $r=1.125$.

trajectory with $2<P$ also has no intersection with the phase denoted by "$P \geqslant 1$." Therefore, when we encode multiple patterns, these networks cannot retrieve pattern no matter how we set pattern frequency ω.

B. The optimal shape of the STDP time window to encode a large number of spatiotemporal patterns

The above-mentioned neural networks cannot memorize multiple spatiotemporal patterns. This small storage capacity of the networks is due to crosstalk effect induced by the large value of $\bar{W}=1-r=0.125$. As shown in Eq. (10), variable b is proportional to $\bar{W}$ and P. Therefore, if $\bar{W}$ is large, increase of P gives rise to rapid increases of variable b. This means that trajectory $(b/|a|, \varphi)$ in Fig. 8 quickly escapes from the retrieval phase denoted by "$P \geqslant 1$" with increase of P.

On the other hand, if we set $r=1$, average $\bar{W}$ takes the zero value, and hence variable b takes the zero value for arbitrary finite P. In this case, we can encode a large number of patterns since point $(b/|a|, \varphi)$ does not move even if we change pattern number P. In Fig. 9(a), we plot storage capacity (the maximum of the number of patterns for successful retrieval) as a function of r. As suggested by our analysis,

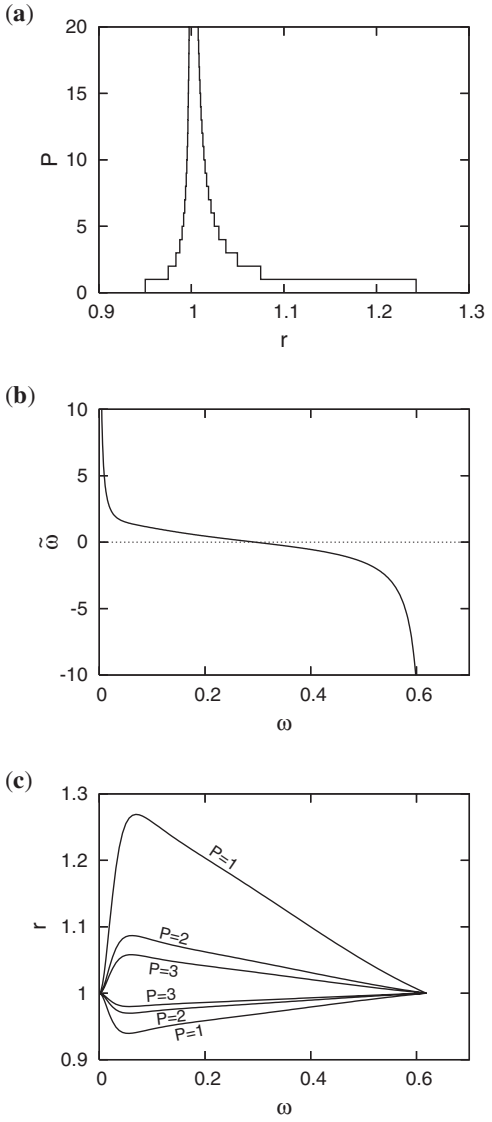

FIG. 9. (a) The storage capacity (the maximum of the number of patterns for successful retrieval) in networks with the learning rule (7)–(10) is plotted as a function of r with parameter $\omega=0.02\times 2\pi$. Storage capacity P^c diverges at $r=1$. The parameters for the time window are set to be the same as Fig. 1 except for r. (b) Setting $r=1$, we plot retrieval frequency of overlap $\tilde{\omega}$ as a function of ω. With $r=1$, retrieval frequency is independent of P. (c) The upper and lower bounds of r for successful retrieval are plotted as a function of ω for $P=1,2,3$. Retrieval state is stable in the region between the upper and the lower bounds for each value of P.

P^c in Fig. 9(a) diverges at $r=1$. The time window with $\bar{W}=0$ is thus optimal to encode a large number of spatiotemporal patterns.

When we set $r=1$, point $(b/|a|, \varphi)$ lies on the X axis of the $\varphi-(b/|a|)$ phase diagram. This point moves along the X axis as pattern frequency ω increases. The change of retrieval frequency $\tilde{\omega}$ during this point movement is plotted in Fig. 9(b) as a function of ω. The retrieval frequency $\tilde{\omega}$ diverges at both the ends since point $(b/|a|, \varphi)$ approaches $(0, -\pi/2)$ or $(0, \pi/2)$ at these ends. Similarly to Fig. 8(b), retrieval frequency $\tilde{\omega}$ in Fig. 9(b) decreases as ω increases. However,

retrieval in Fig. 9(b) is successful in the wider range of ω than that in Fig. 8(b). To investigate how parameter r affects this range of ω, in Fig. 9(c), we plot the upper and lower bounds of r for successful retrieval as a function of ω for the various values of P. In this figure, retrieval is successful in the region between the upper and the lower bounds. As the figure indicates, the range of ω is maximized with $r=1$. At $r=1$, the range of ω is independent of P, while at the different r, the range dramatically decreases as P increases. Therefore, at least in the present model, the time window with $\bar{W}=0$ is effective also in maximizing the range of pattern frequency ω for successful pattern retrieval.

V. DISCUSSION

We have studied STDP-based spatiotemporal learning in analog neural networks. To encode periodic spatiotemporal patterns η_i^μ, we have defined variables a and b by Eqs. (7) and (10), and have introduced learning rule (9). The numerical simulation in Fig. 2 has elucidated that learning rule (9) permits building analog neural networks acting as associative memory for spatiotemporal patterns. The pattern retrieval in this numerical simulation occurs at a different time scale from encoded patterns. To analyze this change of time scale in pattern retrieval, we have derived dynamics of order parameters assuming that pattern number P is finite. An evaluation of the retrieval solution in the order parameter dynamics has clarified that retrieval frequency $\tilde{\omega}$ is a function of the phase of the Fourier transform of time window $W(\Delta t)$. We have also analyzed the stability of the retrieval solution and have shown that the stability of the retrieval state with a single encoded pattern ($P=1$) is determined by two eigenvalues λ_1 and λ_2. However, with multiple encoded patterns ($1<P$), we have found appearance of an additional eigenvalue κ in the stability analysis. This eigenvalue κ suggests the possible phase transition in which stable retrieval state with a single encoded pattern ($P=1$) becomes unstable with multiple patterns ($1<P$). Actually, in Fig. 6, we have found the occurrence of this phase transition due to the eigenvalue κ. In Figs. 8 and 9, we have discussed the influence of the shape of the STDP time window on the retrieval properties. The results in Fig. 9(a) have shown that when the time average of the time window $\bar{W}$ takes the zero value, one can encode the maximal number of spatiotemporal patterns. The analytical results in Fig. 9(c) demonstrates that the time window with $\bar{W}=0$ is effective in maximizing the range of pattern frequency ω for successful retrieval.

Equation (31) shows that variable φ, namely, the phase of variable a, determines retrieval frequency $\tilde{\omega}$. If time window $W(\Delta t)$ is an odd function [i.e., $W(\Delta t)=-W(-\Delta t)$], variable a is a pure imaginary number, and phase φ takes $-\pi/2$ or $\pi/2$. In this case, retrieval is impossible since Eq. (30) shows that $|m^1|$ takes the zero value when $\varphi=\pm\pi/2$. This means that, for successful pattern retrieval, we have to adjust the parameters so that the shape of time window $W(\Delta t)$ deviates from perfect antisymmetry. One possible way to break the antisymmetry is to set $\tau_- \neq \tau_+$ in Eq. (50). We can also control phase φ by changing τ_0 since variable a is proportional to $e^{-i\omega\tau_0}$ as shown in Eq. (51).

On the other hand, if time window $W(\Delta t)$ is an even function [i.e., $W(\Delta t)=W(-\Delta t)$], variable a is a real number, and phase φ takes 0 or π. When variable a is a real number, synaptic connections become symmetric (i.e., $J_{ij}=J_{ji}$). It is well known that when connections are symmetric and the transfer function is a monotonically increasing function, analog neural networks have the Lyapunov function $L(\{x_i\}) = -\frac{1}{2}\Sigma_{ij}J_{ij}v_iv_j+\Sigma_i\int_0^{v_i}F^{-1}(v_i)dv_i$ with $v_i=F(\Sigma_jJ_{ij}x_j)$. This Lyapunov function ensures eventual settlement to a fixed point, and this fact is consistent with $\tilde{\omega}=0$ at $\varphi=0$ in Eq. (31). Kühn *et al.* have pointed out that the existence of a Lyapunov function allows one to use the analytical method based on the equilibrium statistical mechanics since the global minimum of a Lyapunov function can be evaluated by the zero temperature limit of distribution $P(\{x_i\}) \propto \exp[-\beta L(\{x_i\})]$ [17]. Note, however, that when complex number a induces dynamical pattern retrieval, this technique based on the Lyapunov function is unavailable since asymmetric synapse connections make the Lyapunov function useless.

It is an interesting problem to apply the present STDP-based learning rule to spin neural networks. Coolen *et al.* have derived the order parameter dynamics of spin neural networks assuming the asymmetric Hebb learning rule in the Glauber dynamics [7]. If we apply their scheme to neural networks with the STDP-based learning rule, we obtain the order parameter dynamics similar to Eqs. (14) and (16). It is almost evident that the present STDP-based learning rule induces oscillation of an overlap also in spin neural networks.

The P-dependent stability of the present analog neural networks is remarkable in contrast with spin neural networks with the typical Hebb learning rule. In the present associative memory, retrieval state is given as a function of a and b in learning rule (9). Although this retrieval state is independent of P, the linear stability can depend on P owing to eigenvalue κ. Whereas, the properties of retrieval state of spin neural networks with the Hebb rule are always the same as ferromagnetic state for arbitrary finite P. The major cause of P-dependent stability in the present associative memory model seems to be the X term, which appears in local fields owing to parameter b. The Heaviside function assumed in Sec. IV yields positive X. However, if we assume $F(h)=\tanh(\beta h)$, X can take the zero value. The change of the form of transfer function $F(h)$ thus can influence the P-dependent stability. It is also interesting to investigate the effect of b-term to spin neural networks since spin neurons, which take -1 or $+1$, possibly yield the zero-valued X. When variable a is a real number, the b term may give an interesting influence on the stability of the replica symmetric solutions.

The numerical simulations in Figs. 5(b) and 5(c) suggest the presence of mixture state, in which a number of patterns are retrieved simultaneously. The order parameter dynamics (19)–(21) is applicable also to the mixture state. Thus, one can evaluate the stability of the mixture state following the scheme similar to Secs. III C and III D. It is interesting to investigate the influence of noise on the stability of the

mixture state since, in the Hopfield model, adding noise or changing temperature can avoid the network from sticking in the spurious state. We may expect that even when the present neural networks have no energy function, adding noise help destabilizing the mixture state so that the retrieval state has a wider basin of attraction. However, some aspects of the mixture state of the present neural network are different from those of Hopfield model. In the present model, the mixture state of two patterns can be stable as shown in Figs. 5(b) and 5(c), while in the Hopfield model, mixture state of an even number of patterns is unstable. The further analysis is necessary to discuss the stability of mixture state.

Figure 9(a) shows that $r=1$, and hence $\bar{W}=0$, is the optimal condition to encode multiple spatiotemporal patterns in analog neural networks. Also in our previous studies on spiking neural networks, condition $\bar{W}=0$ has been shown to maximize the storage capacity of the networks [9,10]. The analytical solutions in these studies indicate that $\bar{W}=0$ leads to the vanishing of cross-talk effect and divergence of P^c. An interesting fact is that the experimentally found STDP time window, which has both a negative part and a positive part as in Fig. 1, is quite efficient in reducing the size of $\bar{W}$, and hence encoding a large number of spatiotemporal patterns. From the studies of spin neural networks with symmetric connections [3], we expect that with $\bar{W}=0$, the storage capacity of the present neural networks is proportional to N (i.e., $P^c=\alpha^c N$). Actually, under the same condition as Fig. 2, numerical simulations with $N=2000$, 4000, and 8000 suggest the existence of the storage capacity of order N ($P^c \sim 0.02N$). Analytical derivation of this storage capacity of order N, however, requires the further theoretical studies on dynamical pattern retrieval in asymmetric neural networks.

In the present analysis, we only treat the case of the periodic spatiotemporal patterns defined by Eq. (3). However, the STDP-based learning rule (4) is applicable to a considerably wide class of spatiotemporal patterns. Figure 10 describes a result of a numerical simulation in which the STDP-based learning is utilized to encode spatiotemporal Poisson bursting patterns. We generate three random spatiotemporal patterns according to homogeneous Poisson process as shown in Fig. 10(a), and encode the patterns by learning rule (4). Then, in Fig. 10(b), we carry out a numerical simulation setting the initial condition close to the onset activities of the first pattern. Note that the bumps of the analog neuron activities in Fig. 10(b) show an excellent accordance with bursting activities in Fig. 10(a), while the shapes of the bumps in Fig. 10(b) are different from the bursting activities in Fig. 10(a) as in the case of Fig. 2. It is remarkable that in Fig. 10(b) some neurons exhibit multiple bump activities while some other neurons stay in the silent state. It is also worthy to note that after the retrieval finishes, every neuron returns to the silent state. The similar phenomenon is found to occur in spiking neural networks as shown in Fig. 11. These results of the numerical simulations demonstrate the highly flexible applicability of the STDP time window to encoding timings of activities in a variety of neural networks. We will report the further details on the retrieval of the Poisson patterns somewhere else.

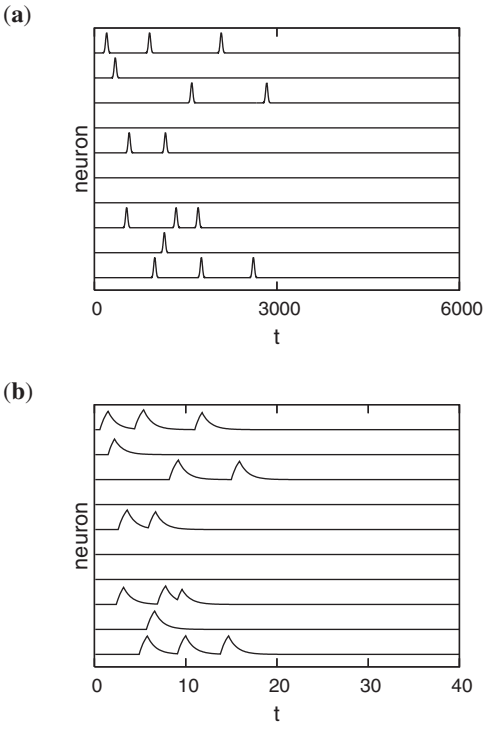

FIG. 10. A numerical simulation of the STDP-based learning of spatiotemporal Poisson bursting activities. (a) We first generate three random spatiotemporal patterns ($\mu=1,\ldots,3$). (a) shows activities of the first ten neurons ($i=1,\ldots,10$) in the first random spatiotemporal pattern ($\mu=1$). Bursting activities in the interval $0 \leqslant t \leqslant 3000$ are generated randomly according to homogeneous Poisson process with a constant rate $\lambda=1/3000$. (b) Second, we encode the three random patterns ($\mu=1,\ldots,3$) by the STDP-based learning rule (4), and carry out a numerical simulation setting the initial condition close to the onset activities of the first pattern ($\mu=1$). (b) shows the first ten neuron activities in the numerical simulation. These behaviors of analog neurons show the excellent accordance with the encoded pattern shown in (a). We model bursting activities in (a) by Gaussian distributions with standard deviation $\sigma=25$. The STDP-based learning is carried out with the same time window as Fig. 1. The numerical simulation in (b) is done with the Heaviside function with the threshold value 0.1 [i.e., $F(h)=H(h-0.1)$]. 10 000 neurons are assumed in both figures.

Both in the present study on analog neural networks and in previous studies on spiking neural networks [9,10,29,30], the STDP induces retrieval of spatiotemporal patterns at a different time scale than encoded patterns. The present study shows that analog neural networks with positive φ exhibit the negative retrieval time scale, at which retrieval occurs in reverse order. Interestingly, such reversed replay of spatiotemporal activities has been observed in the electrophysiological experiments in the Hippocampus of awaking rats [31]. The normal order replay of spatiotemporal patterns has also been found to occur at a faster time scale in sleeping rats [32]. Our studies of spatiotemporal associative memories contribute to a systematic understanding of the variety of time scales in spatiotemporal replays in the real nervous system.

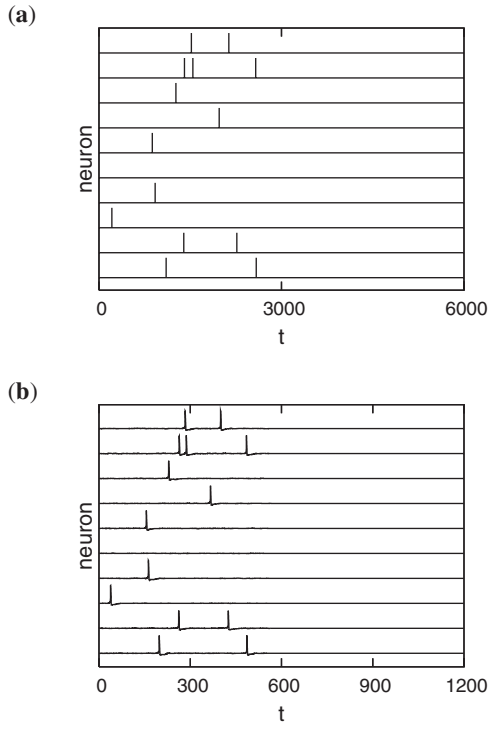

FIG. 11. The same as Fig. 10, but spiking neural networks are assumed instead of analog neural networks. Spiking neurons are modeled by the Hodgkin-Huxley equations, and interconnected by chemical synapses. (a) The activities of the first ten neurons in the first random pattern ($\mu=1$). In the interval $0\leqslant t\leqslant 3000$, delta-function-like activities (spike timings) are generated randomly according to the homogeneous Poisson process. (b) The behaviors of the first ten spiking neurons in the numerical simulation, where the initial part of the first spike pattern ($\mu=1$) is evoked by the pulsed external inputs at $t=0$. These behaviors of the spiking neurons also show the excellent accordance with the encoded spike pattern shown in (a).

ACKNOWLEDGMENT

The authors thank Dr. Cojocaru for his fruitful comments on our manuscript.

APPENDIX: ANALYTICAL SOLUTIONS FOR ANALOG NEURAL NETWORKS WITH THE HEAVISIDE FUNCTION

The analysis in Sec. III covers analog neural networks with arbitrary transfer function $F(h)$. The purpose of the present section is to use the Heaviside function $H(h)$ in Eq. (48) to derive the specific analytical solutions for the Heaviside function.

Before conducting stability analysis, we have to calculate retrieval state with the Heaviside function. Substitution of Eq. (48) into Eq. (25) yields

$$|m^1| = \frac{1}{2\pi}\int_0^{2\pi} \cos\phi^1 H[|a||m^1|\cos(\phi^1+\varphi)+bX]d\phi^1$$

$$= \frac{1}{2\pi}\int_0^{2\pi} \cos(\phi^1-\varphi) H[|m^1|\cos\phi^1 + (b/|a|)X]d\phi^1,$$

$$= \frac{1}{2\pi}\left[\int_0^{\phi_0} \cos(\phi^1-\varphi)d\phi^1 + \int_{2\pi-\phi_0}^{2\pi} \cos(\phi^1-\varphi)d\phi^1\right]$$

$$= \frac{1}{\pi}\cos\varphi\sin\phi_0, \tag{A1}$$

where we define ϕ_0 as

$$\phi_0 = \cos^{-1}\left(-\frac{(b/|a|)X}{|m^1|}\right). \tag{A2}$$

In the same manner, Eq. (27) is rewritten in the form

$$X = \frac{\phi_0}{\pi}. \tag{A3}$$

With $b=0$, we can easily solve Eqs. (A1)–(A3), to obtain $\phi_0=\pi/2$, $X=1/2$, and $|m^1|=(1/\pi)\cos\varphi$. When variable b takes a nonzero value, we reduce Eqs. (A1)–(A3), further and obtain the following two equations:

$$|m^1| = \frac{1}{\pi}\cos\varphi\sin(\pi X) \tag{A4}$$

and

$$\cos(\pi X) = -\frac{(b/|a|)X}{|m^1|}. \tag{A5}$$

Therefore, X satisfies the equation

$$X = -\frac{\cos\varphi}{2(b/|a|)\pi}\sin(2\pi X). \tag{A6}$$

The numerical solution of the above equation determines X. Then, we can obtain $|m^1|$ from Eq. (A4).

To evaluate stability condition with $P=1$, we calculate eigenvalues of matrix $\mathbf{A}$ in Eq. (36). Substituting $H'(h)=\delta(h)$ into Eq. (33), we obtain

$$I(\xi^1, a\xi^1) = \frac{1}{2\pi}\int_0^{2\pi} \cos\phi^1 \delta[|a||m^1|\cos(\phi^1+\varphi)+bX]$$
$$\times|a|\cos(\phi^1+\varphi^1)d\phi^1$$
$$= \frac{1}{2\pi}\int_0^{2\pi} \cos(\phi^1-\varphi)\delta(|a||m^1|\cos\phi^1+bX)$$
$$\times|a|\cos\phi^1 d\phi^1$$
$$= c(2|a|\cos^2\phi_0\cos\varphi), \tag{A7}$$

where

$$c = 1/(2\pi|a||m^1|\sin\phi_0). \tag{A8}$$

In the same manner, we obtain

$$I(\xi^1, b) = c(2b\cos\phi_0\cos\varphi), \tag{A9}$$

$$I(1, a\xi^1) = c(2|a|\cos\phi_0), \tag{A10}$$

and

$$I(1, b) = c(2b). \tag{A11}$$

Therefore, matrix $\mathbf{A}$ takes the form

$$\mathbf{A} = \begin{pmatrix} -1 + c(2b) & c(2|a|\cos\phi_0) \\ c(2b\cos\phi_0\cos\varphi) & -1 + c(2|a|\cos^2\phi_0\cos\varphi) \end{pmatrix}. \tag{A12}$$

Eigenvalues of matrix **A** are given as

$$\lambda_1 = -1 \tag{A13}$$

and

$$\lambda_2 = -1 + \frac{1}{\pi|m^1|\sin(\pi X)}[\cos^2(\pi X)\cos\varphi + (b/|a|)], \tag{A14}$$

where we replace ϕ_0 by πX using Eq. (A3). From these eigenvalues, we can evaluate the stability condition (37).

Finally, we compute eigenvalue κ to analyze the stability for the case of multiple patterns $(1 < P)$. Following the same manner as Eqs. (A7)–(A11), we obtain

$$I(\xi^2, a\xi^2) = c(|a|\cos\varphi). \tag{A15}$$

Therefore, eigenvalue κ in Eq. (46) is computed as

$$\kappa = -1 + \frac{1}{2\sin^2(\pi X)}, \tag{A16}$$

where we use Eqs. (A1) and (A3). From eigenvalue κ as well as eigenvalues λ_1 and λ_2, we can evaluate the stability condition (47)

[1] J. J. Hopfield, Proc. Natl. Acad. Sci. U.S.A. **79**, 2554 (1982).
[2] D. J. Amit, H. Gutfreund, and H. Sompolinsky, Phys. Rev. A **32**, 1007 (1985).
[3] D. J. Amit, H. Gutfreund, and H. Sompolinsky, Phys. Rev. Lett. **55**, 1530 (1985).
[4] S. Amari, IEEE Trans. Comput. **C-21**, 1197 (1972).
[5] N. Matsumoto and M. Okada, Neural Comput. **14**, 2883 (2002).
[6] H. Sompolinsky and I. Kanter, Phys. Rev. Lett. **57**, 2861 (1986).
[7] A. C. C. Coolen and T. W. Ruijgrok, Phys. Rev. A **38**, 4253 (1988).
[8] W. Gerstner, R. Ritz, and J. L. van Hemmen, Biol. Cybern. **69**, 503 (1993).
[9] M. Yoshioka, Phys. Rev. E **65**, 011903 (2001).
[10] M. Yoshioka, Phys. Rev. E **66**, 061913 (2002).
[11] S. Scarpetta, L. Zhaoping, and J. Hertz, Neural Comput. **14**, 2371 (2002).
[12] S. Scarpetta and M. Marinaro, Hippocampus **15**, 979 (2005).
[13] J. Cook, J. Phys. A **22**, 2057 (1989).
[14] A. Arenas and C. J. P. Vicente, Europhys. Lett. **26**, 79 (1994).
[15] T. Aoyagi and K. Kitano, Phys. Rev. E **55**, 7424 (1997).
[16] M. Yoshioka and M. Shiino, Phys. Rev. E **61**, 4732 (2000).
[17] R. Kühn, S. Bös, and J. L. van Hemmen, Phys. Rev. A **43**, 2084 (1991).
[18] S. Amari and K. Maginu, Neural Networks **1**, 63 (1988).
[19] J. Phys. A **22**, 1959 (1989), special issue in memory of Elizabeth Gardner (1957–1988).
[20] H. Nishimori, T. Nakamura, and M. Shiino, Phys. Rev. A **41**, 3346 (1990).
[21] J. Hertz, A. Krogh, and R. G. Palmer, *Introduction to the Theory of Neural Computation* (Perseus Books Group, New York, 1991).
[22] M. Shiino and T. Fukai, J. Phys. A **25**, L375 (1992).
[23] M. Okada, Neural Networks **8**, 833 (1995).
[24] H. Markram, J. Lübke, M. Frotscher, and B. Sakmann, Science **275**, 213 (1997).
[25] G. Q. Bi and M. M. Poo, J. Neurosci. **18**, 10464 (1998).
[26] L. I. Zhang, H. W. Tao, C. E. Holt, W. A. Harris, and M. M. Poo, Nature (London) **395**, 37 (1998).
[27] G. Q. Bi and M. M. Poo, Annu. Rev. Neurosci. **24**, 139 (2001).
[28] Y. Kuramoto, *Chemical Oscillations, Waves, and Turbulence* (Springer-Verlag, Berlin, 1984).
[29] M. Yoshioka, Phys. Rev. E **71**, 061914 (2005).
[30] M. Yoshioka, Phys. Rev. E **71**, 065203(R) (2005).
[31] D. J. Foster and M. A. Wilson, Nature (London) **440**, 680 (2006).
[32] Z. Nádasdy, H. Hirase, A. Czurkó, J. Csicsvari, and G. Buzsáki, J. Neurosci. **19**, 9497 (1999).